frontiers | Frontiers in Physics

TYPE Original Research
PUBLISHED 31 January 2025
DOI 10.3389/fphy.2024.1527389

OPEN ACCESS

EDITED BY
Qiuqin Sun,
Hunan University, China

REVIEWED BY
Changgang Li,
Shandong University, China
Haoxi Cong,
North China Electric Power University, China

*CORRESPONDENCE
Lezhi Ou,
oulezhi@126.com

RECEIVED 13 November 2024
ACCEPTED 09 December 2024
PUBLISHED 31 January 2025

CITATION
Wang C, Ou L, Wu W, Tan C, Ding Y and Zou J (2025) Measurement of electromagnetic transients in high voltage substations based on wireless transmission technique under strong electromagnetic interference. *Front. Phys.* 12:1527389. doi: 10.3389/fphy.2024.1527389

Measurement of electromagnetic transients in high voltage substations based on wireless transmission technique under strong electromagnetic interference

Ceyong Wang, Lezhi Ou*, Wenbing Wu, Chenghui Tan, Yi Ding and Jinxing Zou

State Grid Hunan Xiangdian Test and Research Institute Co., Ltd., Changsha, China

As power grids expand, the insulation performance of electrical equipment becomes crucial for grid reliability. Thus, measuring transient voltage and current at key substation nodes is essential. Traditional methods are cumbersome and pose electric shock risks with faulty grounding. To address this problem, a wireless-based electromagnetic transient measurement method is proposed in this paper. Firstly, distributed intelligent sensors are placed at various substation points for on-site intelligence. Secondly, a compression algorithm with fault tolerance prevents signal distortion. Then, a distributed wireless synchronous sampling strategy ensures accurate sampling under varying conditions. Finally, field tests show the system achieves high accuracy.

KEYWORDS

electromagnetic transients, wireless transmission technique, electromag netic interference, intelligent sensor, signal acquisition

1 Introduction

Operating experience with power systems demonstrates that the insulation properties of high-voltage equipment, such as transformers and disconnectors, are crucial for the reliable operation of the power grid. When the power system experiences a failure or operational change, its parameters shift dramatically, causing a rapid transition from one operating state to another. This process is often accompanied by transient overvoltage and overcurrent events that cause serious damage to electrical equipment [1]. To promptly identify and address defects and potential hazards in time, and ensure the safe, reliable, and stable operation of the substation, it is essential to collect and analyze the transient voltage and current waveforms of high-voltage equipment. Traditional acquisition usually relies on wired mode, i.e., the voltage and current signals distributed in different positions are centrally connected to the recorder through long-distance pay-off for manual test recording. However, the method has some problems such as cumbersome connection to the test line and the possibility of electric shock when the ground terminal is defective [2]. Furthermore, the inefficiency of wired collection means is low, and it is difficult to meet the test needs of large-scale power grids, which restricts the development of field tests.

Nowadays, with the rapid development of wireless sensor network technology, and the wide application of computer technology, wireless acquisition systems have attracted much attention [3–5]. Currently, wireless communication technologies such as BLE Bluetooth communication technology, Zigbee communication technology, NB-IoT narrowband Internet of Things technology, and LoRa communication technology have become common choices [6]. These wireless acquisition systems and their sensor networks can be widely deployed in various parts of the power grid, such as power plants, substations, and transmission lines [7]. Ref. [8] proposed a remote system for continuous monitoring of ground and leakage currents in high-voltage substations based on wireless LAN technology, which is characterized by low power consumption and built-in overvoltage protection. Ref. [9] studied the reliability of Zigbee-based wireless sensor network technology in transforming traditional power systems into smart grids, and expounds its limitations and challenges in application. A real-time situational awareness framework for power transmission networks was developed using wireless sensor networks in Ref. [10] and its feasibility under current technical conditions was verified. A power quality detection node based on Zigbee technology was designed in [11], which effectively solved the drawbacks of wired communication and realized remote wireless monitoring of power quality.

The current technologies and methods have played an active role in improving the effectiveness, applicability and reliability of wireless data acquisition in power systems. However, in the strong electromagnetic interference of substation, there are still some problems that need to be solved, such as poor anti-error ability of wireless network data transmission and system time out-of-step. Therefore, an improved RLE data compression and distributed wireless synchronous sampling control are proposed to solve the problems in this paper. Furthermore, a transient voltage and current measurement and analysis system based on wireless transmission is designed and developed.

2 Sensors and wireless transmission technique

2.1 Principle of intelligent sensor

Traditional power sensors are usually divided into electromagnetic and capacitive types. The operating principle is to convert high-voltage signals into small signals that can be processed. There are various types of sensors, such as the use of capacitive voltage divider and the small signal optical fibers. Among them, the capacitive voltage dividers are widely used in the field of high-voltage testing due to better dynamic, excellent linearity and simple construction. Since the secondary side is not fully isolated from the primary side, there is a risk of electric shock if the secondary side is inadequately grounded. The voltage transformer uses an inductive structure, but its limited bandwidth may cause core saturation, leading to inaccuracies in the overvoltage signal. Fiber optic voltage transformers are isolated by photoelectric coupling, which improves insulation and electrical isolation, and its accuracy can meet the needs of transient signal acquisition. However, the optical fibers are vulnerable to damage and breakage, which is not suitable for application in substation.

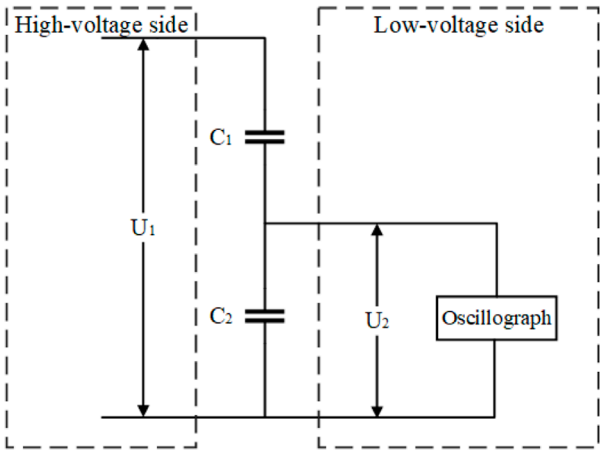

FIGURE 1
Equivalent circuit diagram of capacitive voltage divider. C_1 and C_2 are the capacitance of the high-voltage and low-voltage side, respectively; U_1 and U_2 are the voltage of the high-voltage and low-voltage side, respectively.

The methods of transient voltage and current acquisition of high-voltage electrical equipment in substations are mainly divided into direct and indirect methods. Direct measurement of transient voltage generally relies on capacitive voltage division, with the signal testing conducted directly through the end screen of bushing. The schematic diagram of the signal acquisition used in our study is shown in Figure 1.

The relationship of U_1 and U_2 can be expressed by Equation 1,

$$\frac{U_1}{U_2} = \frac{(C_1 + C_2)}{C_2} \tag{1}$$

2.2 Wireless sensor network

Wireless sensor network (WSN) is a distributed self-organizing sensor network that integrates embedded computer, sensing technology and wireless communication. The perception layer of the wireless sensor network is composed of a sensing node deployed on the object to be detected and a convergence node that gathers all information, and the perception network formed by the above two nodes has two structures, as shown in Figure 2. For the network structure, the signals obtained by the sensing node reach the convergence node in the mode of multi-hop transmission. Regarding to the star structure, the signals reach the convergence node in the mode of point-to-point transmission.

There are several kinds of wireless network communication, such as Bluetooth, ZigBee, Z-Wave, etc. Compared with Bluetooth, ZigBee and Z-Wave, LoRa has advantages in terms of transmission rate, communication distance, and cost performance [12, 13]. The number of sensors in IoT has increased greatly in recent years, and almost every product needs to be connected to many sensing nodes. Some wireless transmission technologies are no longer able to be used for WSN deployment due to their own limitations. Low power

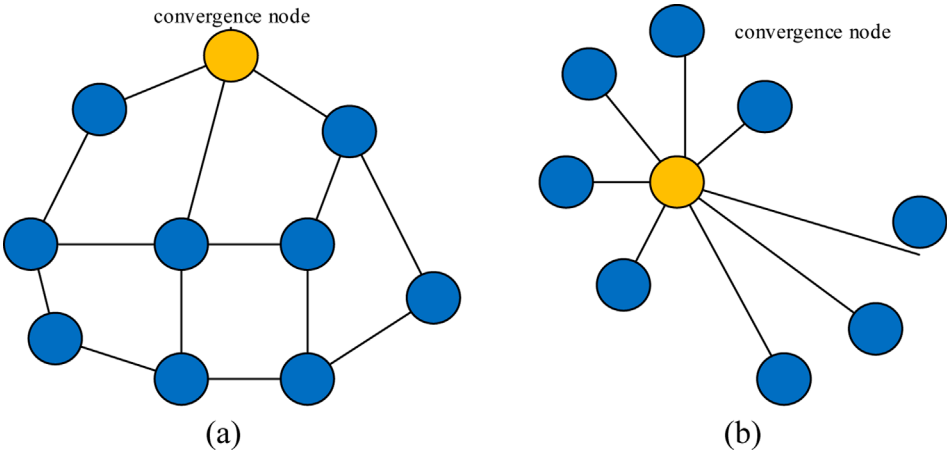

FIGURE 2
Network structure of sensing layer of wireless sensor network. **(A)**reticulated structure. **(B)** star structure.

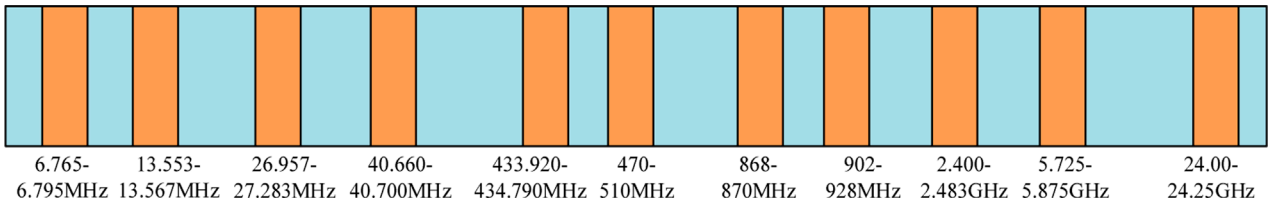

FIGURE 3
ISM band division standard.

wide area networks (LPWAN) are capable of transmitting data over long distances, and support connecting a huge number of nodes, due to their lower power consumption and bandwidth. LPWANs are generally divided into two types: licensed and unlicensed spectra. LoRa operates in the range of 137 MHz–1,020 MHz, which covers the ISM RF band of the radio classification standard, which has no specific restrictions and can be used by anyone. The ISM distribution in China is shown in Figure 3, and LoRa is deployed in the frequency band from 470 to 510 MHz. Therefore, LoRa can achieve a long-distance communication up to 8 km in the city, and even reach more than 20 km in the suburbs.

Generally, digital signals are modulated into analogue signals during transmission. There are three techniques are often used in signal modulation, such as frequency shift keying (FSK), amplitude shift keying (ASK) and phase shift keying (PSK). Unlike above modulation techniques, LoRa uses spread spectrum for signal modulation. The principle involves using a spread spectrum coding function on the transmitter side to modulate the information into a wideband signal, while the corresponding function on the receiver side compresses and demodulates the received signal. The modulation waveform equation is expressed by Equation 2,

$$s(t) = \sqrt{\frac{2E_X}{T_b}} \cos\left(2\pi f_0 t \pm 2\pi \frac{\Delta F}{T_b} t^2\right) \quad (2)$$

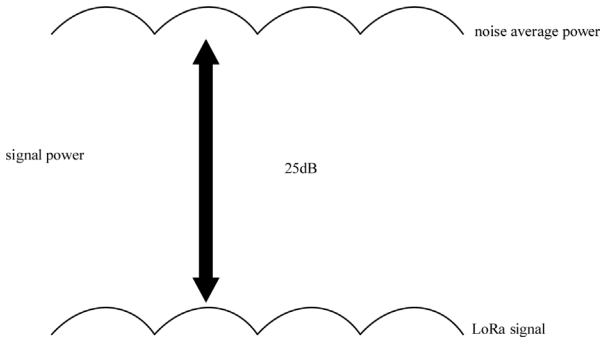

FIGURE 4
Comparison of LoRa signal and noise average power.

where E_x and T_b are the energy of the transmitted signal and the signal duration, respectively; f0 is the carrier frequency; ΔF is the frequency difference of the pulse.

Even with noise interference, the receiver can successfully recover the information transmission. As shown in Figure 4, the LoRa signal can be successfully received at 25 dB below the noise average power.

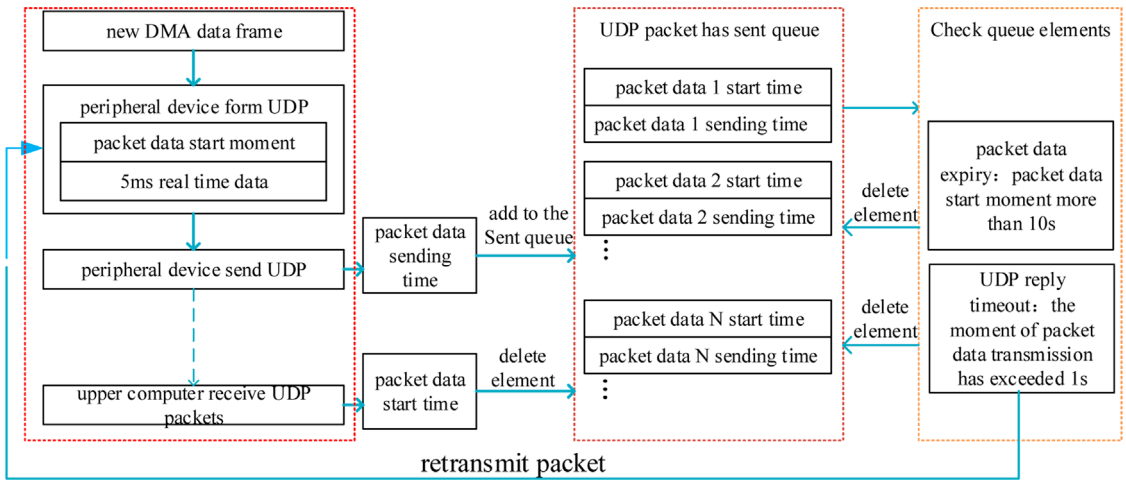

FIGURE 5
Block diagram of real-time waveform transmission and fault tolerance implementation.

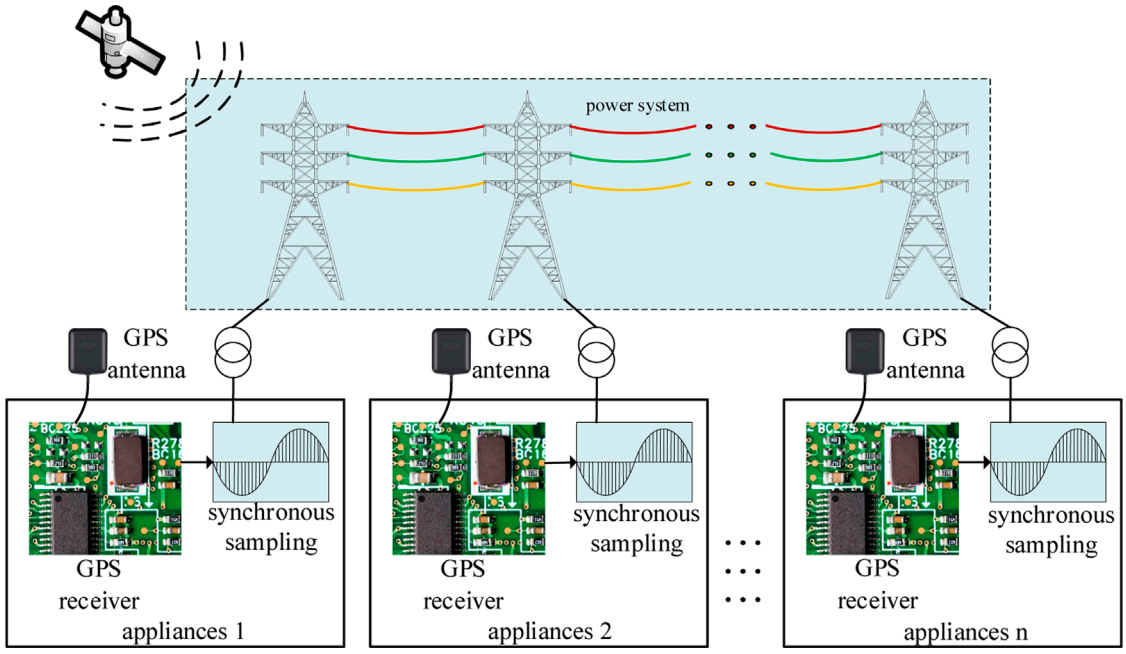

FIGURE 6
Architecture of distributed synchronous sampling system.

2.3 Wireless signal transmission technique under strong electromagnetic interference

2.3.1 Error-resistant wireless transmission

To enhance the reliability of large data transmission in wireless networks operating in strong electromagnetic interference, the run length encoding (RLE) algorithm is used. It primarily compresses consecutive occurrences of the same elements by replacing them with the element itself and the count of its repetitions. This approach improves both compression efficiency and speed [14]. The algorithm compresses consecutive repeated data by replacing identical data points with a single data point followed by the count of repetitions. It can effectively reduce the redundancy of data and lower the size of data. Moreover, it is simple to implement and offers fast decompression, making it well-suited for real-time transmission and processing requirements [15]. The data to be encoded can be a one-dimensional data stream or multidimensional, such as an image or volumetric data. For industrial frequency data waveforms, the use of RLE compression algorithm is simple and effective. To improve the characteristics of industrial frequency waveform data, the traditional RLE algorithm may not be able to achieve the optimal compression effect [16]. Adaptive threshold-based

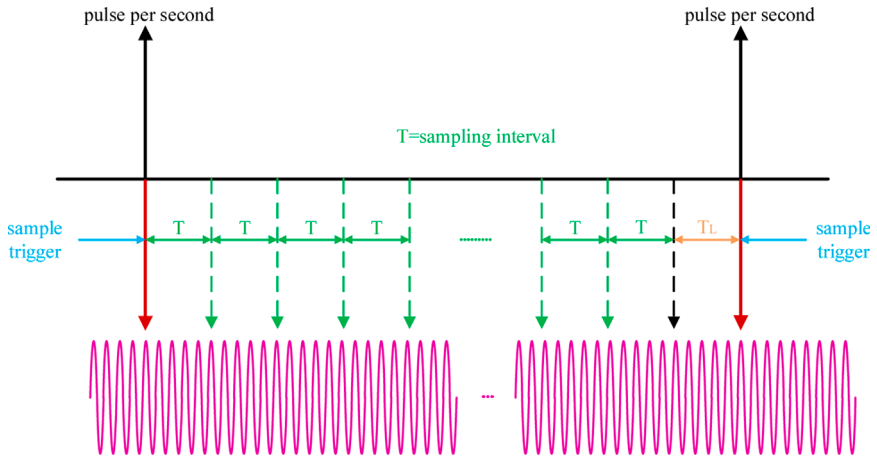

FIGURE 7
Schematic diagram of PPS-based synchronized mascot harvesting.

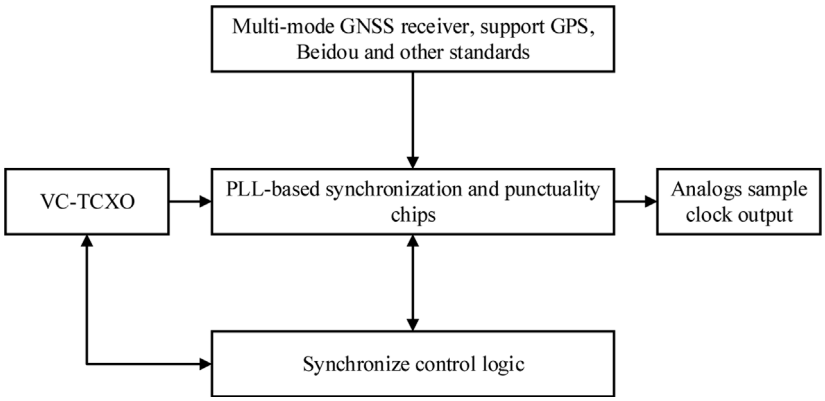

FIGURE 8
Structure of clock synchronization system.

chunking strategy is used, which dynamically adjusts the chunk size according to the changes in the data, and divides consecutive identical data sequences into the same data chunks, to make better use of the advantages of the RLE algorithm.

The specific implementation method flow as follows:

(1) Data pre-processing: the original waveform data are firstly cleaned to remove outliers, noise and other interfering factors. For the missing values, choose the appropriate filling method according to the data characteristics (e.g., use the value of the previous valid data point, average value or interpolation, etc.).
(2) Characteristic analysis: analyses the variation characteristics of the IF waveform data, including periodicity, amplitude variation range, frequency components, etc. Identify repetitive patterns or similar waveform segments in the data, which are usually the parts that can be effectively compressed by the RLE algorithm.
(3) Adaptive chunking: determine the appropriate chunk size based on the results of data characteristic analysis. For highly periodic data, the chunk size can be associated with the cycle length. For non-periodic data or mutated parts of the data, a smaller chunk size can be used to capture more details of the changes. Dynamically adjust the chunking strategy to accommodate changes in the data. For example, when a significant change in the data pattern is detected, the chunk size can be re-evaluated and adjusted.
(4) RLE compression: the RLE algorithm is applied independently within each data chunk. The RLE algorithm compresses data more efficiently because of the higher similarity of data within a data block. Record the metadata (e.g., block size, starting position, etc.) of each data block so that the original data can be accurately restored during decompression.

The retransmission mechanism is used to improve the reliability of data transmission. Moreover, identification information is added to the packet to avoid sending the same packet repeatedly, such as sequence number or timestamp. The Block diagram of real-time waveform transmission and fault tolerance implementation is shown in Figure 5.

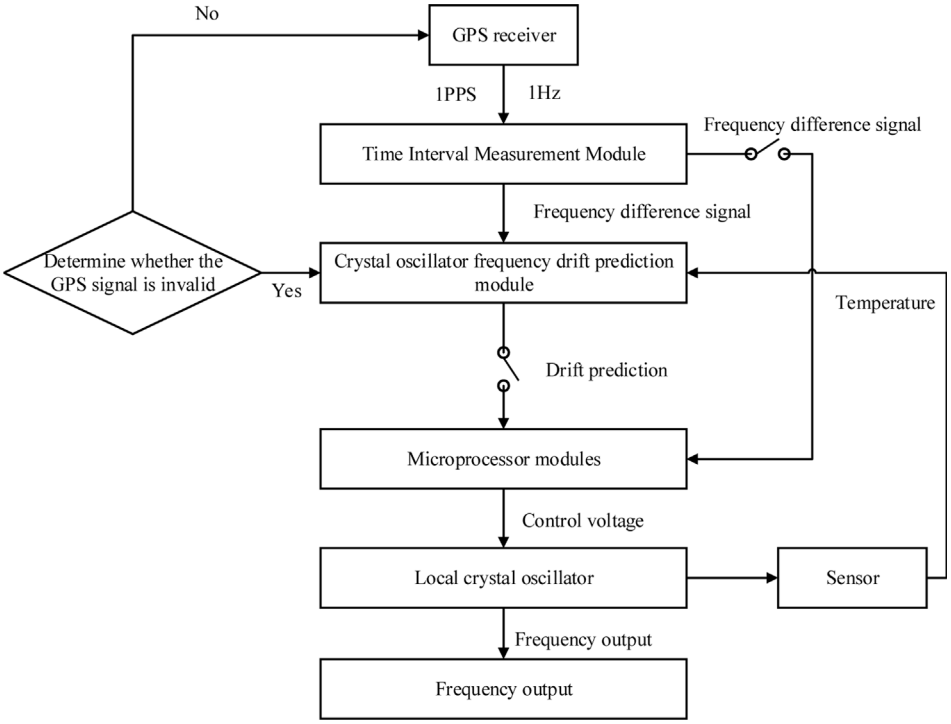

FIGURE 9
Schematic diagram of the frequency of the crystal oscillator based on GPS signal calibration.

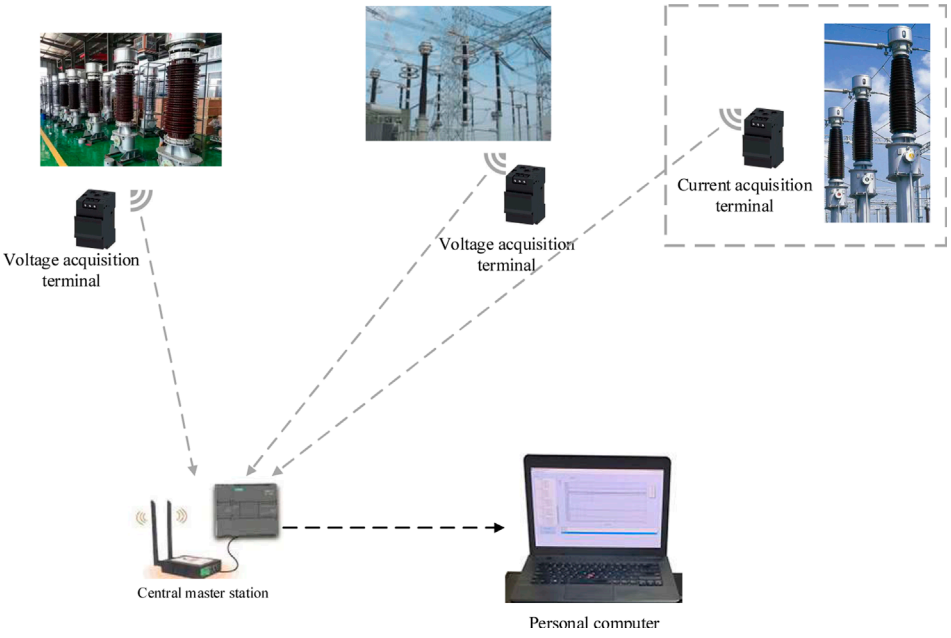

FIGURE 10
Wireless synchronous acquisition system.

2.3.2 Distributed wireless synchronized sampling control strategy

The collection terminals for voltage, current, etc., are distributed in different locations within the substation. Each terminal node needs to strictly synchronize the time to ensure consistent timing of data acquisition. Currently, the most widely used timing approach is GNSS timing, which can reach several tens of nanoseconds in accuracy. The pulse per second (PPS) edge generated by the global

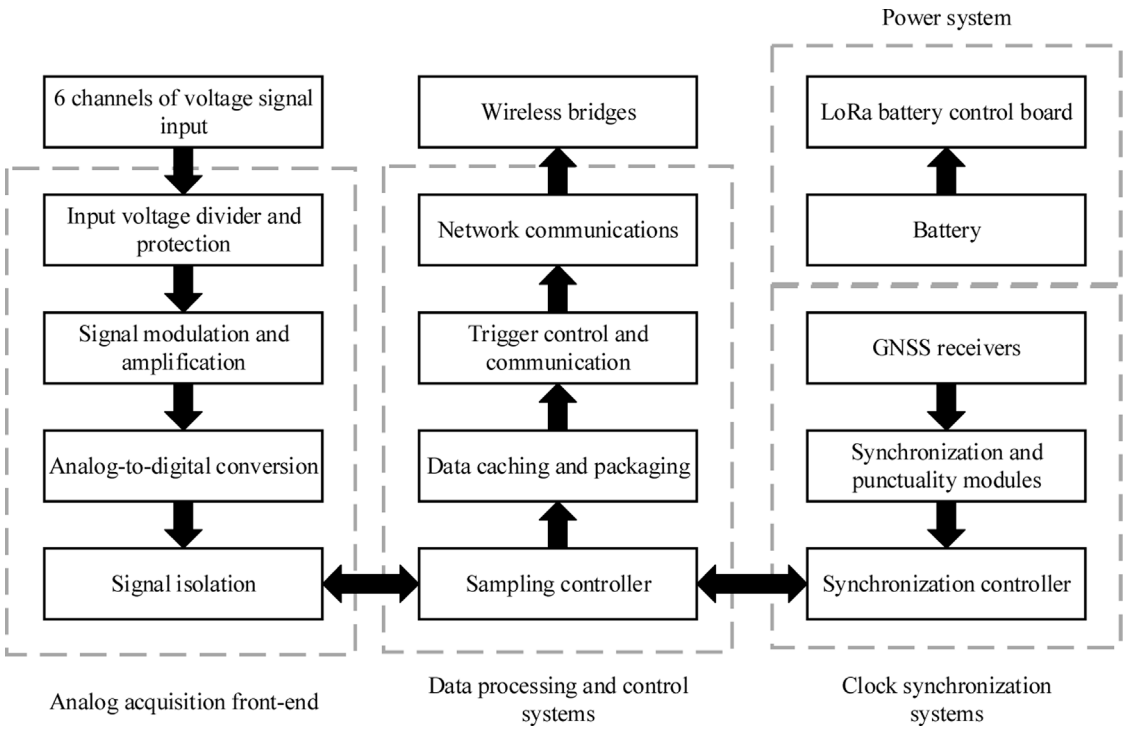

FIGURE 11
Overall architecture of hardware.

navigation satellite system (GNSS) receiver module is typically used as the synchronization signal to initiate data acquisition each second, after which coordinated universal time (UTC) is appended to the data. The traditional architecture of distributed synchronous acquisition is shown in Figure 6.

As shown in Figure 6, the acquisition terminal receives GPS satellite signals and generates PPS signals through the GPS antenna. The PPS edge is used as a synchronization signal by the acquisition control module to complete data acquisition, as shown in Figure 7. It adds UTC timestamps to the data and utilizes time alignment at the centralized data terminal to achieve synchronization of the sampled waveform data. However, differences in the frequency and temperature coefficients of the crystal oscillators in the sampling control modules of each acquisition terminal may cause errors in the uniform interval durations, potentially leading to the accumulation of these errors over time. Eventually, these errors would cause the phase difference between the sampled data points at the end of different acquisition terminals to exceed the acceptable range. Under the complex electromagnetic environment, the signal of the GNSS timing may be lost, leading to the system time out of step.

To solve the above problem, the signal of GNSS timing combined with a self-holding clock based on digital phase-locked loop technology (PLL) are taken as the time reference of the acquisition terminal. As shown in Figure 8, the clock synchronization system is composed of multi-mode GNSS receiver, high precision voltage-controlled temperature-compensated crystal oscillator (VCTCXO), PLL-based synchronous timing circuit and so on. The clock synchronization system is used to provide timing reference for the acquisition terminal to ensure synchronous sampling.

Under the influence of aging and temperature, the crystal frequency basically presents a quadratic curve change, which can be expressed by Equation 3,

$$x_{(t)} = a + bt + \frac{1}{2}bt^2 + \varepsilon_{x_{(t)}} \tag{3}$$

where $x_{(t)}$ represents the clock difference drift of crystal oscillator under the influence of aging and temperature, and the unit is s; a represents the relative shift of crystal frequency at zero time. b represents the frequency shift at zero time; c stands for linear migration; $\varepsilon_{x_{(t)}}$ represents the random component, i.e., the deviation of the crystal frequency caused by other factors.

Take the derivative of Equations 3, 4 can be expressed,

$$y_{(t)} = b + ct + \varepsilon_{y_{(t)}} \tag{4}$$

where $y_{(t)}$ represents the instantaneous frequency deviation of crystal oscillator in ppm; $\varepsilon_{y_{(t)}}$ represents the corresponding random variation component.

Clearly, the random component of the instantaneous frequency shift in crystal vibration cannot be described by a fixed formula and can only be predicted statistically based on the frequency shift representation of the crystal vibration. Based on the above analysis, the fundamental principle of the frequency of the crystal oscillator based on GPS signal calibration is depicted in Figure 9. Firstly, the influence of aging, temperature and other factors on the frequency drift of crystal oscillator is analyzed. The model of frequency drift prediction is established. The state likelihood function and state equation are derived. Then, the diffusion parameters are estimated by maximum likelihood estimation method and the drift parameters

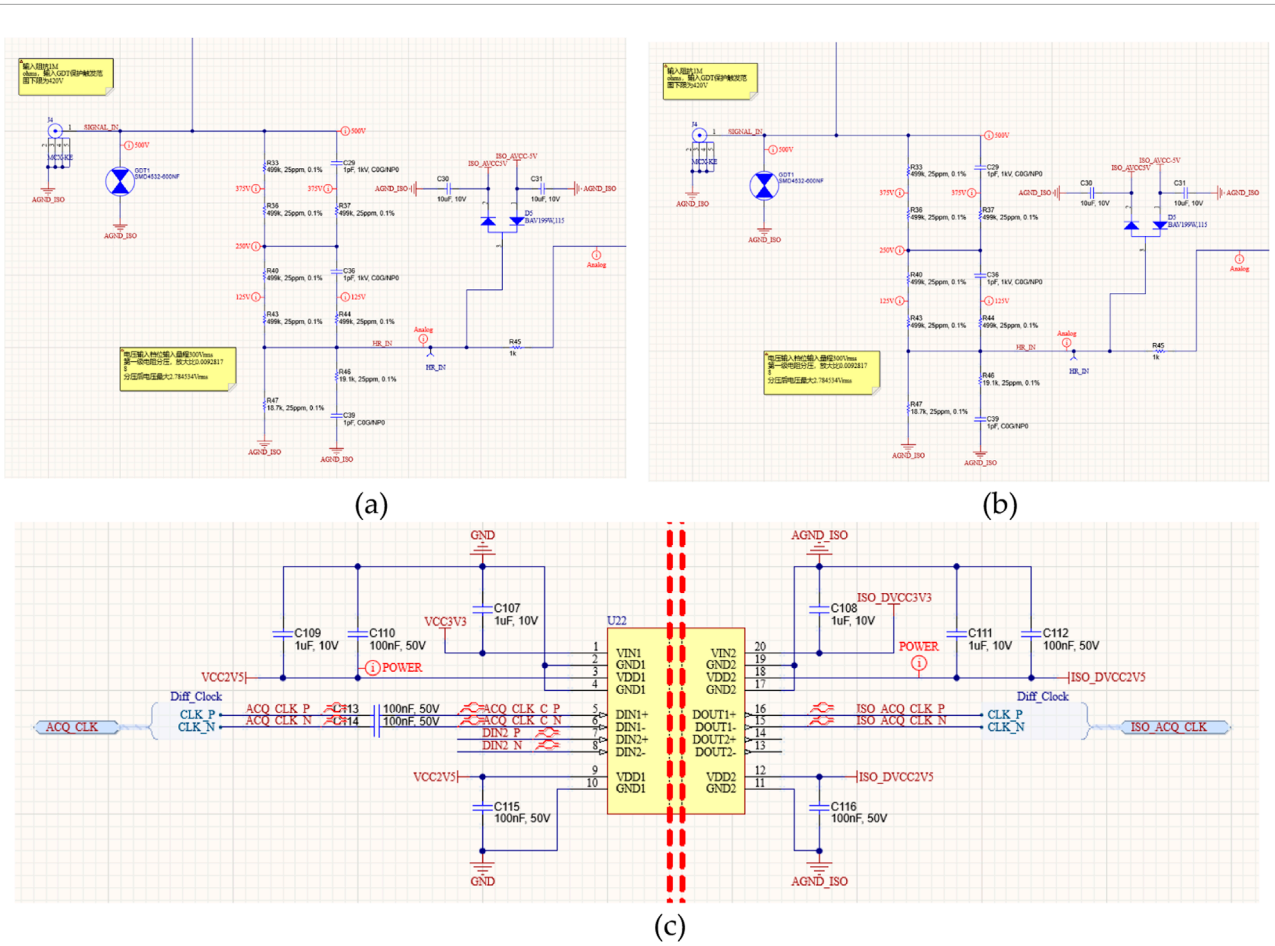

FIGURE 12
Electric circuit for signal acquisition terminals. **(A)** analog circuit for voltage divider; **(B)** signal isolation circuit; **(C)** ADC sampling and clock isolation circuit.

are estimated by Kalman filter algorithm. According to the derived frequency drift prediction formula, the output frequency drift of crystal oscillator is calculated. Finally, the predicted crystal oscillator output frequency drift is converted into a control voltage source to adjust the crystal oscillator output frequency in real-time to achieve high precision frequency output of the system.

In the case of GNSS signal is valid, the synchronous sampling control method based on the signal of GNSS timing is adopted. Once the GNSS signal is disabled by strong electromagnetic interference, the system automatically switches to the PLL-based synchronous timing, independently running GNSS backup clock. The system automatically switches the input signal of the synchronous clock according to the running status of the GNSS clock by the synchronous clock arbitration mechanism. The PLL-based synchronous timing circuit takes the local high-precision VCTCXO as the reference, controls the internal PLL to synchronize with the input reference PPS, and outputs the output PPS signal and sampling reference clock synchronized with the input reference PPS. High precision (sub-microsecond) wireless time synchronization in strong electromagnetic environment can be achieved by combining the primary synchronization signal with the backup synchronization signal.

3 Experiment study

3.1 Experiment setup

The wireless synchronous acquisition system is composed of four parts: voltage acquisition terminal, current acquisition terminal, central master station and analysis host computer, as shown in Figure 10. The system uses 5.8GHzWifi wireless LAN to realize data acquisition and interaction. 470 MHz LORA wireless network is used to realize the work control. The obtained data from the terminals as well as the control task signals are exchanged from the central master station to the analysis host computer through the WLAN.

3.1.1 Voltage or current acquisition terminals

Voltage or current acquisition terminals, installed at sampling points, facilitate high-speed signal acquisition, real-time measurement of steady-state parameters, and monitoring of transient processes. When a transient value exceeds its threshold, the terminal records waveform data from both before and after the event and uploads it in real-time to the analysis host for processing.

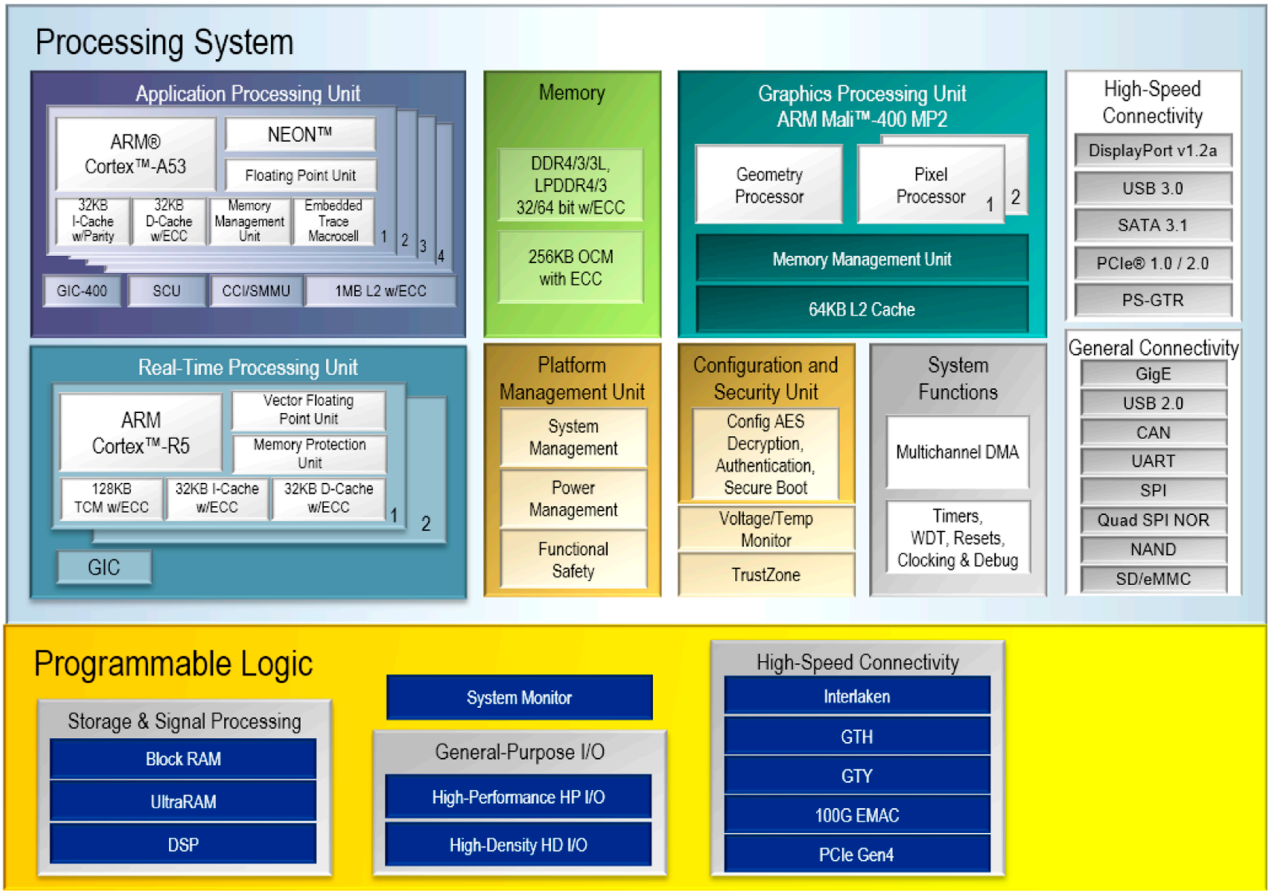

FIGURE 13
The structure of Xilinx Zynq UltraScale + Soc.

If any monitoring terminal detects a transient anomaly, it triggers synchronized sampling across all terminals in the system.

3.1.2 Central master station

The central master station manages wireless network deployment and synchronously triggers control functions. The system uses a dual-frequency network for seamless communication between data collection terminals and analysis hosts. To ensure reliable data transmission across widely dispersed monitoring terminals, the communication host connects with acquisition terminals via a 5.8 GHz wireless network, while the main station communicates with the analysis host using a 2.4 GHz WIFI network. In field applications, remote power on/off operations are implemented to reduce energy consumption. A 470 MHz low-power wireless control network is established between the supervisory station and data collection terminals to support remote power switching.

3.1.3 Analysis host computer

It is a system-level human-machine interaction device. By means of wireless local area network, it connects to the central main station, enabling control tasks to be dispatched and data exchanges between terminals.

The tested voltage signal may originate from either the secondary side of the transformer (PT) or the voltage signal obtained after voltage division conversion from the primary high-voltage circuit. In this paper, the voltage terminal input signal design is for 0–300 V voltage input, which can be directly connected to the secondary signal of a PT; the voltage will be measured from the termination point of the transformer winding, with plans to employ an existing capacitor voltage divider box (the rated voltage division results in a signal control within 10 V). In the test system, the current acquisition signal is the secondary side signal of the CT. To capture high-frequency signals in transient currents and low-frequency signals in surges, current sensors employ wide-band clamp-type current sensors.

3.2 System design

The wireless synchronous acquisition system consists of analog acquisition component, data processing and control system, clock synchronization system, power supply system and wireless bridge. As shown in Figure 11, the analog acquisition is responsible for processing the input analog signal and converting it into digital signal. The data processing and control

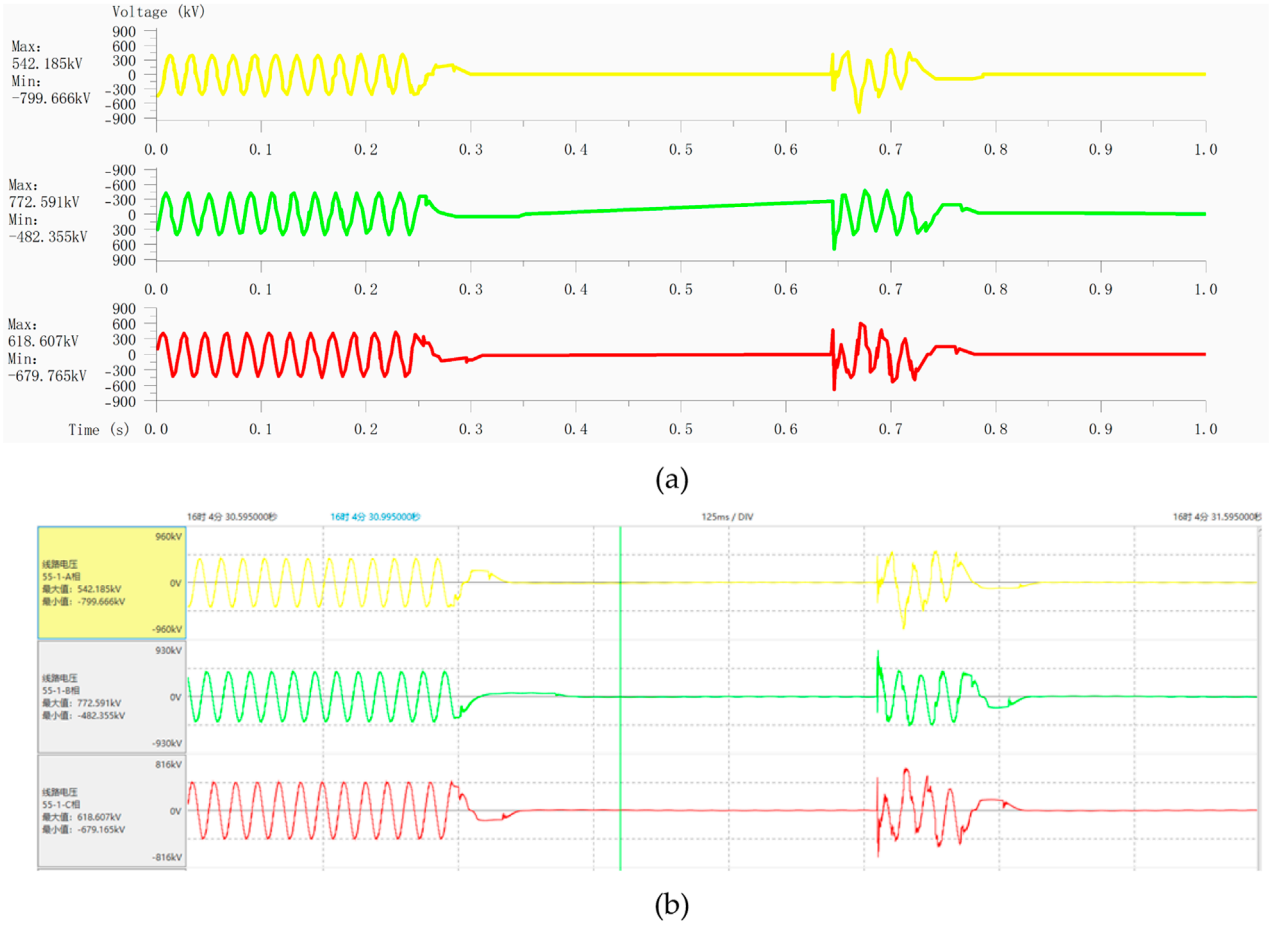

FIGURE 14
Voltage waveform during line switching. **(A)** Wireless synchronous acquisition system; **(B)** on site.

system is the core of the whole system, responsible for data collection, trigger control, communication with the analysis host computer and data storage. The clock synchronization system receives satellite timing information to achieve clock synchronization. The power supply system realizes the power supply of the system and remote power switch control based on LoRa. The wireless bridge provides a physical wireless network connection between the terminal and the central station. Electric circuit for signal acquisition terminals is shown in Figure 12.

As depicted in Figure 12, the simulated acquisition frontend is intended to realize 300Vrms AC voltage input by employing resistive voltage division, converting high-voltage signals into low-voltage signals that can be measured by the ADC. To ensure the bandwidth of the voltage divider circuit, high-voltage and low-voltage arms are interconnected with RC compensation loops, compensating for any bandwidth loss incurred due to parasitic capacitance or inductance of the voltage division resistors. At the input terminal of the signal, a gas discharge tube was installed with an action voltage of 600 V to prevent transient high-voltage inputs from causing damage to the equipment. A diode is paralleled at the input of the low-voltage signal to suppress transient overvoltage and prevent damage to the subsequent low-voltage circuit. The ADC segment is expected to employ a high-precision 16 bit, 2 Mbps ADC, ensuring optimal measurement accuracy and dynamic range for the device. The bandwidth of simulated signal chain exceeds 200 kHz, effectively reducing high-frequency signal attenuation and distortion. A high-speed, multi-channel electromagnetic isolation chip is considered for signal isolation.

The proposed sampling rate for voltage recording terminal is 2 Msps, which corresponds to an immense increase in data processing volume. This paper intends to employ an SoC processor based on Xilinx Zynq UltraScale+, as illustrated in Figure 13. An AXI interconnect internal bus is employed for high-speed communication between Field-Programmable Gate Array (FPGA) and a CPU, concurrently relieving the CPU of data retrieval load by utilizing AXI Direct Memory Access (DMA) mode for ADC sampling data transfer to the CPU. This enables non-blocking data transport from the FPGA to system memory without occupying the CPU. The AXI bus connecting the CPU and FPGA is configured with a 32-bit/100 MHz specification, delivering a speed of 3.2 Gbps, which is ample to meet the real-time transmission requirements for six-channel sampling data.

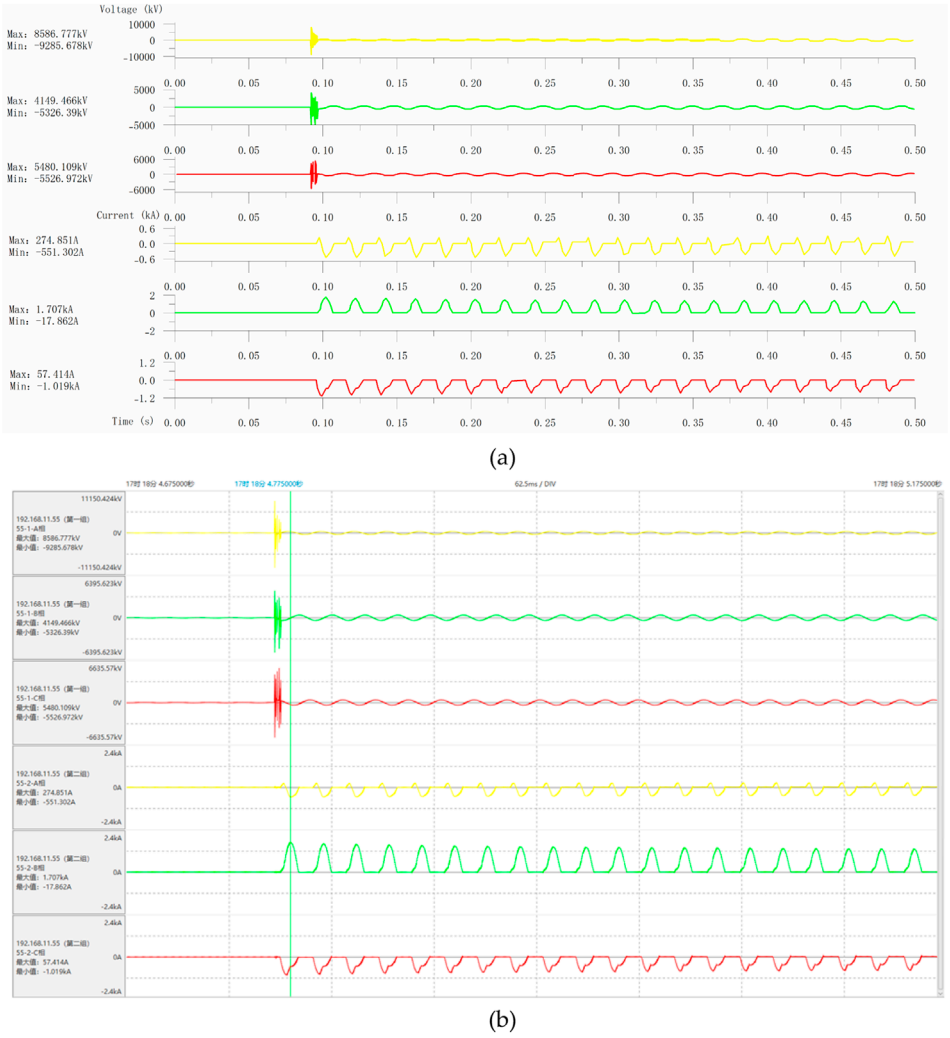

FIGURE 15
Voltage and current waveform while switching on transformer. **(A)** Wireless synchronous acquisition system; **(B)** on site.

4 Field test

The operation of transmission line, power transformer, reactive power compensation equipment, and filter bank in a substation are carried out.

4.1 Switching transmission line

Auto-reclosing is a common strategy for transmission line used to improve the reliability of power supply. It can reduce the impact of power supply interruption in the case of transient faults. The line is firstly cleared at t = 0.836 s, then reclosed at t = 1.232 s, and finally switched off from the system again at t = 1.305. The voltage and current in this process are measured in field test, as depicted in Figure 14. The peak value of the A-phase overvoltage reaches 799.666 kV in reclosing process. Those for phase B and C are relatively small. During the closing process, the current suddenly increases, causing energy to be exchanged between inductance and capacitance of the line. This results in oscillations and the generation of overvoltage. The peak of the voltage oscillation decays very faster, and the time constant is small. The peak of the closing overvoltage has statistical characteristics, and its value is affected by various factors, e.g., the closing phase angle, the residual charge, and the number of outgoing lines connected to the busbar.

4.2 Switching power transformer

When switching a power transformer into service, the saturation of the iron core produces a very high current, with an amplitude much larger than the normal load current, as shown in Figure 15. It is the so-called inrush current. The peak of overcurrent for phase B is 1.707 kA and that for phase C is 1.019 kA. The waveform for the inrush current is spiky, and distinct from the sinusoidal waveform. Its frequency is low and mainly concentrated in the vicinity of power frequency 50 Hz. While switching on power transformer, the voltage fluctuation is also very significant. The system voltage experiences a great distortion. The overvoltage depends on the phase angle of

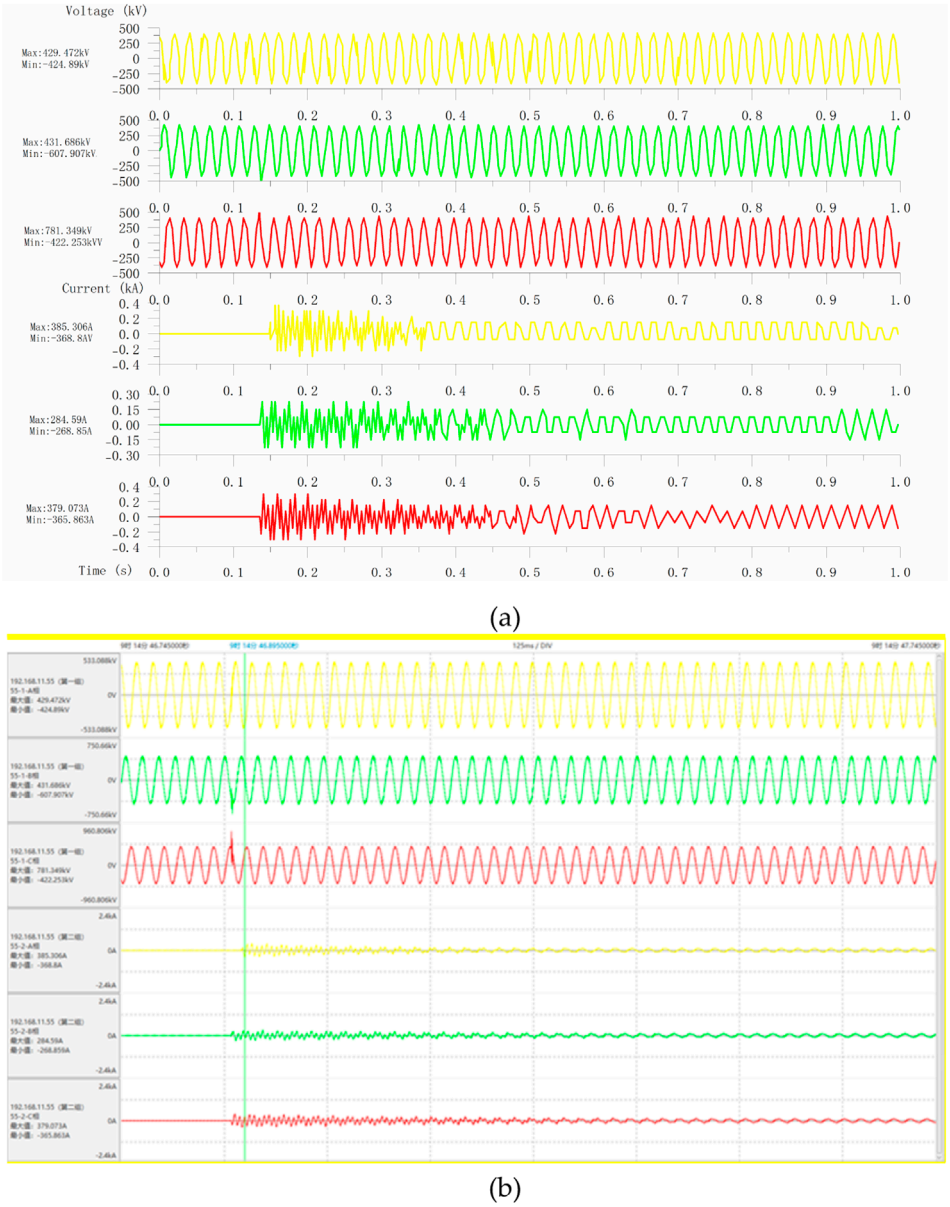

FIGURE 16
Bus voltage and branch current while switching off reactive power compensation. **(A)** Wireless synchronous acquisition system; **(B)** on site.

the closing and can compromise the insulation strength of power equipment to some extent.

4.3 Switching reactive power compensation equipment

Reactive power compensation plays a key role in power systems by improving the power factor, reducing losses in power supply transformers and transmission lines, enhancing supply efficiency, and improving the overall power supply environment. The reactive power compensation equipment is indispensable. The optimization of reactive power compensation can minimize the power grid loss, smooth voltage fluctuations and reduce the harmonics. A set of field tests are conducted in a substation installed with reactive power compensation equipment. The bus voltage as well as the branch is measured, as shown in Figure 16. Clearly, the peak overvoltage of phase A, phase B and phase C of the bus are 429.47, 607.91 and 781.35 kV, respectively. In terms of the branch current of reactive power compensation device, the overcurrent of phase A, phase B and phase C are 385.31, 284.59 and 379.07 A, respectively.

4.4 Switching filter bank

Both the bus voltage and filter current are measured while switching off a set of filter bank of a substation, as shown in Figure 17. The filter is cleared at t = 26.622 s. In this

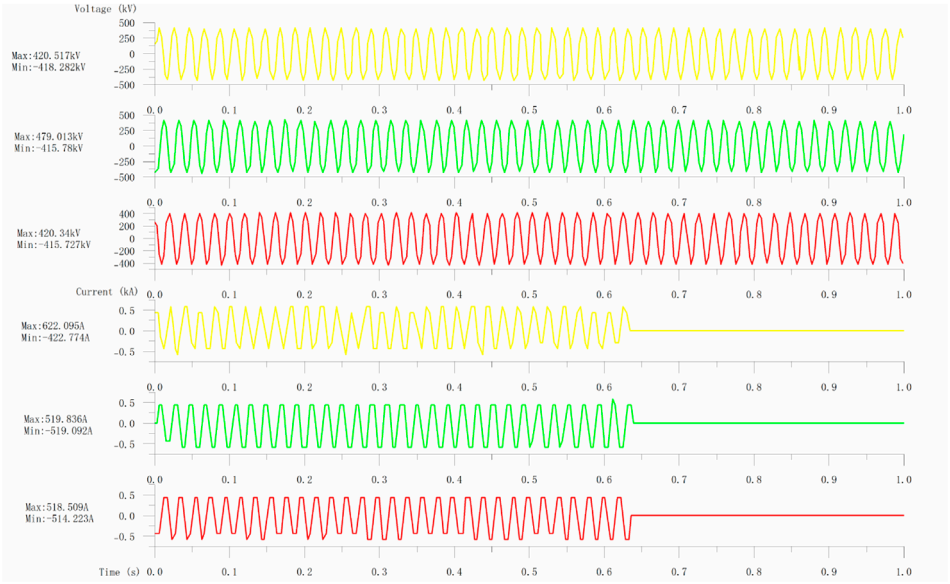

(a)

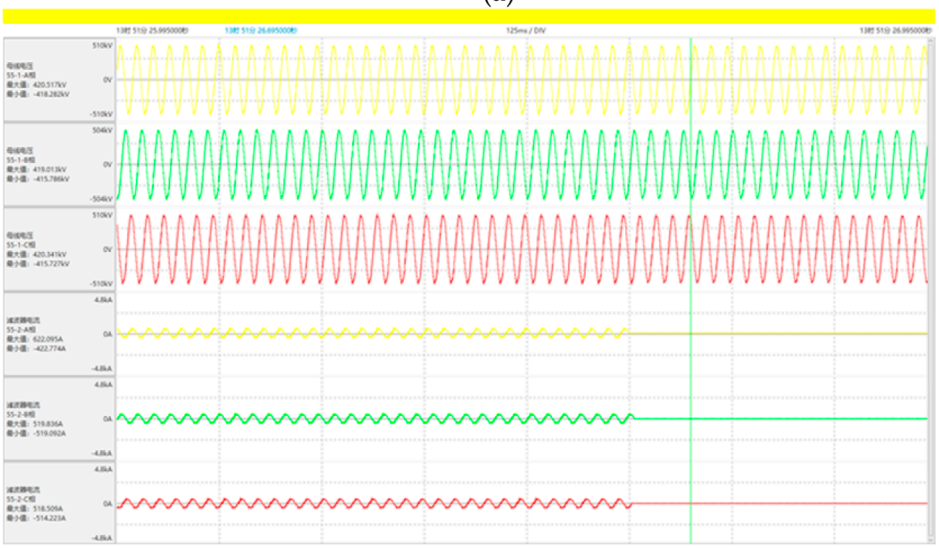

(b)

FIGURE 17
Bus voltage and branch current while switching off filter bank. **(A)** Wireless synchronous acquisition system; **(B)** on site.

process, the peak value of the overvoltage at phase A is measured 420.52 kV; the peak value of phase B is 419.01 kV; the peak value of phase C is 420.34 kV. Besides, the peak value of phase A, phase B and phase C current are 622.10, 519.83, and 518.51 A, respectively. By measuring the transient voltage and current during these operations, the effectiveness of the transient voltage and current measurement system based on wireless transmission technology in a strong magnetic field environment at the substation was verified. It demonstrates that the system has a high accuracy and can measure the voltage and current signals. It is mainly due to its internal high-precision data acquisition terminal and precise data processing algorithm. It can work stably under various environmental conditions whether high temperature and strong electromagnetic interference. The system is very convenient to install and no wiring is required. It not only saves the cost and time of wiring, but also greatly improves the flexibility and expandability of the system.

5 Conclusion

To address signal distortion, a REL compression algorithm enhanced by a block-based strategy with an adaptive threshold is

proposed. Additionally, a waveform transmission and fault tolerance mechanism are implemented for reliable data transmission.

The GNSS backup clock using a digital PLL resolves system time deviation. A distributed wireless synchronized sampling and control system is developed to ensure high-precision time synchronization under complex operating conditions.

A transient voltage and current acquisition system for substations based on wireless technology is designed. It measures transient currents and voltages during operations such as switching transmission lines, transformers, filters, and reactive power devices, to verify the reliability of the wireless synchronous acquisition system.

Data availability statement

The datasets presented in this study can be found in online repositories. The names of the repository/repositories and accession number(s) can be found in the article/supplementary material.

Author contributions

CW: Writing–original draft, Writing–review and editing, Conceptualization, Data curation, Formal Analysis, Funding acquisition, Investigation, Methodology, Project administration, Resources, Software, Supervision, Validation, Visualization. LO: Writing–original draft, Writing–review and editing. WW: Conceptualization, Investigation, Software, Writing–review and editing. CT: Conceptualization, Data curation, Formal Analysis, Investigation, Writing–original draft. YD: Data curation, Formal Analysis, Methodology, Project administration, Validation, Writing–review and editing. JZ: Formal Analysis, Project administration, Supervision, Validation, Writing–review and editing.

Funding

The author(s) declare that financial support was received for the research, authorship, and/or publication of this article. This work is financially supported by State Grid Hunan Xiangdian Test and Research Institute Co., Ltd (XDKY-2023-07). The funder was not involved in the study design, collection, analysis, interpretation of data, the writing of this article, or the decision to submit it for publication.

Conflict of interest

Authors CW, LO, WW, CT, YD, and JZ were employed by State Grid Hunan Xiangdian Test and Research Institute Co., Ltd.

Generative AI statement

The author(s) declare that no Generative AI was used in the creation of this manuscript.

Publisher's note

References

1. Wu X, Wang A. Harmonic signal processing method based on the windowing interpolated DFT algorithm. *J Inf Sci Eng* (2015) 31(3):787–98.

2. Li J, Liu B, Wang N, Li B, Song J. Wireless transmission technology based operating overvoltage collection and analysis system. *Northeast Electric Power Technology* (2024)(04) 18–22.

3. Gungor VC, Lu B, Hancke GP. Opportunities and challenges of wireless sensor networks in smart grid. *IEEE Trans Ind Electronics* (2010) 57(10):3557–64. doi:10.1109/tie.2009.2039455

4. Parikh PP, Sidhu TS, Shami A. A comprehensive investigation of wireless LAN for IEC 61850–based smart distribution substation applications. *IEEE Trans Ind Inform* (2012) 9(3):1466–76. doi:10.1109/tii.2012.2223225

5. Egan D. The emergence of ZigBee in building automation and industrial controls. *Comput Control Eng* (2005) 16(2):14–9. doi:10.1049/cce:20050203

6. Mahmood A, Javaid N, Razzaq S. A review of wireless communications for smart grid. *Renew Sustainable Energy Rev* (2015) 41:248–60. doi:10.1016/j.rser.2014.08.036

7. Kurt S, Yildiz HU, Yigit M, Tavli B, Gungor VC. Packet size optimization in wireless sensor networks for smart grid applications. *IEEE Trans Ind Electronics* (2016) 64(3):2392–401. doi:10.1109/tie.2016.2619319

8. Harid N, Bogias AC, Griffiths H, Robson S, Haddad A. A wireless system for monitoring leakage current in electrical substation equipment. *IEEE Access* (2016) 4:2965–75. doi:10.1109/access.2016.2577553

9. Sallabi FM, Gaouda AM, El-Hag AH, Salama MMA. Evaluation of ZigBee wireless sensor networks under high power disturbances. *IEEE Trans Power Deliv* (2013) 29(1):13–20. doi:10.1109/tpwrd.2013.2290300

10. Fateh B, Govindarasu M, Ajjarapu V. Wireless network design for transmission line monitoring in smart grid. *IEEE Trans Smart Grid* (2013) 4(2):1076–86. doi:10.1109/tsg.2013.2241796

11. Chen Z, Ouyang M, Liu H. Design of power quality detection node based on ZigBee. *Low Voltage Electr Appliances* (2011)(09) 37–40.

12. Zhou Q, Zheng K, Hou L, Xing J, Xu R. Design and implementation of open LoRa for IoT. *IEEE Access* (2019) 7:100649–57. doi:10.1109/access.2019.2930243

13. Zheng J, Wang T. Optimization research and application of RLE image compression algorithm. *Computer Knowledge Technology* (2014)(25) 5981–4.

14. Robinson AH, Cherry C. Results of a prototype television bandwidth compression scheme. *Proc IEEE* (1967) 55(3):356–64. doi:10.1109/proc.1967.5493

15. Yang S, Hu C, Li H. Wiener process-based frequency guarding method for GPS calibration of crystal-type frequency sources. *China Meas and Test* (2016) 42(6).

16. Partovibakhsh M, Liu G. An adaptive unscented Kalman filtering approach for online estimation of model parameters and state-of-charge of lithium-ion batteries for autonomous mobile robots. *IEEE Trans Control Syst Technology* (2014) 23(1):357–63. doi:10.1109/TCST.2014.2317781